Publishing House
AKAPIT

COMPUTER METHODS IN MATERIALS SCIENCE

Informatyka w Technologii Materiałów

Vol. 15, 2015, No. 1

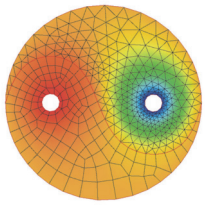

CYCLIC SHEAR BEHAVIOR OF AUSTENITIC STAINLESS STEEL SHEET

BERT GEIJSELAERS*, TON BOR, PETER HILKHUIJSEN, TON VAN DEN BOOGAARD

Universiteit Twente, Engineering Technology,
POBox 217, 7500AE Enschede, Netherlands
**Corresponding author: h.j.m.geijselaers@utwente.nl*

Abstract

An austenitic stainless steel has been subjected to large amplitude strain paths containing a strain reversal. During the tests, apart from the stress and the strain also magnetic induction was measured to monitor the transformation of austenite to martensite. From the in-situ magnetic induction measurements an estimate of the stress partitioning among the phases is determined.

When the strain path reversal is applied at low strains, a classical Bauschinger effect is observed. When the strain reversal is applied at higher strains, a higher flow stress is measured after the reversal compared to the flow stress before reversal. Also a stagnation of the transformation is observed, meaning that a higher strain as well as a higher stress than before the strain path change is required to restart the transformation after reversal.

The observed behavior can be explained by a model in which for the martensitic transformation a stress induced transformation model is used. The constitutive behavior of both the austenite phase and the martensite is described by a Chaboche model to account for the Bauschinger effect. In the model mean-field homogenization of the material behavior of the individual phases is employed to obtain a constitutive behavior of the two-phase composite. The overall applied stress, the stress in the martensite phase and the observed transformation behavior during cyclic shear are very well reproduced by the model simulations.

Key words: metastable austenite, deformation induced martensite, constitutive model

1. INTRODUCTION

Transformation of retained austenite under mechanical loading is especially prominent in austenitic stainless steel. Under the right circumstances, the metastable austenite transforms to martensite under mechanical loading. For recent experimental studies see for example Lebedev and Kosarchuk (2000), Nagy et al. (2004), Post et al. (2008).

Austenitic stainless steels have a broad range of applications. In general, they have high corrosion resistance, high cryogenic toughness, high work hardening rate, high hot strength, high ductility, high hardness, an attractive appearance and low maintenance. The delayed cracking of stainless steel products is in general attributed to the presence of martensite combined with residual stress (Berrahmoune et al., 2006). For the prediction of martensite fraction and residual stresses it is important to have reliable models.

Olson and Cohen (1975) formulated a kinetic model which explains the martensite formation from ε-phase nucleation on shear band intersections during plastic deformation Venables (1962). This *strain induced* kinetic model for martensitic phase transformation has been combined by Stringfellow et al. (1992) with a mean-field homogenization model to obtain overall visco-plastic behavior from the constitutive behavior of the individual phases. Also the influence of the stress state and transformation plasticity were added. Further extensions have been provided by Tomita and Iwamoto (1995) for strain rate dependence and by Diani and Parks (1998) for crys-

ISSN 1641-8581

tal plasticity. Han et al. (2004) added stress dependence by evaluating the mechanical driving force on individual martensite variants. This enabled them to calculate the texture of the resulting martensite.

An alternative theory for mechanically induced martensite formation was proposed by Tamura (1982). In his model the driving force of the applied stress is considered as the reason for the transformation. See also Perdahcıoğlu et al. (2008a). When the thermodynamic driving force as defined by Patel and Cohen (1953) exceeds a threshold value, the transformation will start. Applications of stress induced transformation models suitable for macro scale simulations have been presented by Hallberg et al. (2007) and Perdahcıoğlu and Geijselaers (2012) for austenitic steel and by Lani et al. (2007), Delannay et al. (2008) and Kubler et al. (2011) for TRIP steel.

For accurate prediction of the state of the material after forming, it is important that the non-proportional deformation behaviour is captured correctly. Very few studies of the large amplitude cyclic and non-proportional response of metastable austenitic stainless steel are available in literature. An extensive experimental program, including tension-compression tests, was conducted by Spencer et al. (2009) on austenitic steel. They report a strong Bauschinger effect in the austenite stress-strain response. Results from cyclic shear tests and tensile tests followed by shear tests were presented by Gallée et al. (2007). They formulated a model based on Stringfellow et al. (1992). Hamasaki et al. (2014) showed that observations during large amplitude cyclic tension-compression tests cannot be captured by the strain induced transformation model.

In this paper we report on cyclic shear tests, which have been conducted on a low Carbon 12Cr9Ni4Mo austenitic stainless steel. During the testing the martensite transformation was monitored by a magnetic induction sensor.

A constitutive model of austenitic steel which undergoes a mechanically induced transformation will be presented, where the martensitic transformation is modeled as a stress-driven process similar to the model of Tamura (1982). This transformation model is then combined with a mean-field formulation for description of the constitutive behavior of the two-phase composite.

2. EXPERIMENTS

The material used in the tests is 12Cr9Ni4Mo austenitic stainless steel. Its nominal composition is given in table 1. Specimens were cut from 0.5 mm thick sheet as described in Perdahcıoğlu et al. (2008b) for deformation in shear, which was applied at a rate of approximately 0.001 s^{-1}. The strain was measured real-time on the material surface using a camera and dot-tracking software. Dots were applied to the specimen surface before the test and the corresponding positions were recorded with a frequency of approximately 10 s^{-1}. The data was averaged and post-processed to find the 2-dimensional deformation tensor **F** in the material from which the shear strain γ_{xy} is calculated.

Table 1. *Chemical composition of the 12Cr9Ni4Mo steel used in the experiments in wt.%.*

C+N	Cr	Ni	Mo	Cu	Ti	Al	Si
<0.05	12.0	9.1	4.0	2.0	0.9	0.4	<0.5

During the cyclic shear tests the magnetic induction was measured to monitor the course of the martensitic transformation. Post et al. (2008) give calibration data for this specific sensor. For this paper however the raw sensor readings will be of more interest than the actual martensite volume fractions. The magnetic induction value is subject to the Villari effect, it depends on the applied stress. This has been shown for tensile stresses by for example Post et al. (2008) and Maréchal et al. (2012). It also appears when a shear stress is applied. Moreover, the effect of the shear stress is symmetric with respect to zero stress. This offers the possibility to determine the strain and stress at which, during the strain reversal, a zero shear stress in the martensite is reached. In this way the partitioning of the stress between both phases can be estimated.

3. EXPERIMENTAL RESULTS

The measured shear stress vs. shear strain data are shown in figure 1 and the absolute values of the stresses vs. cumulative strains are plotted in figure 2. It is clearly seen, that after strain reversal reyielding starts at a distinctly lower stress than was attained before strain reversal. This indicates that the material behavior of the austenite has a strong Bauschinger effect, which agrees with the findings of Spencer et al. (2009). The tests with considerable transformation before strain reversal show that soon after reyielding a stress level is reached, which exceeds the stress level before reversal.

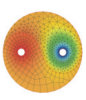

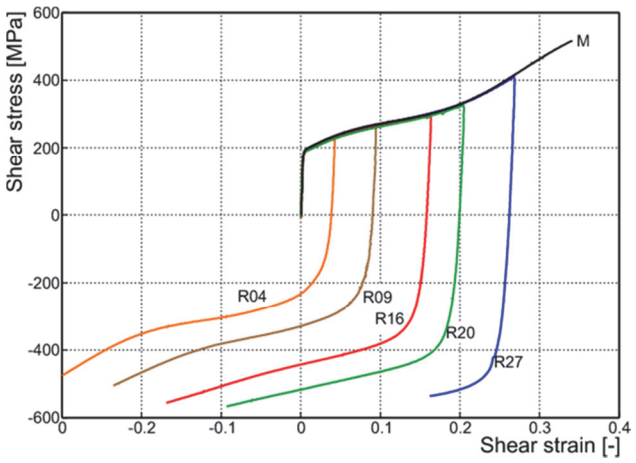

Fig. 1. Shear stress versus shear strain during cyclic shear tests.

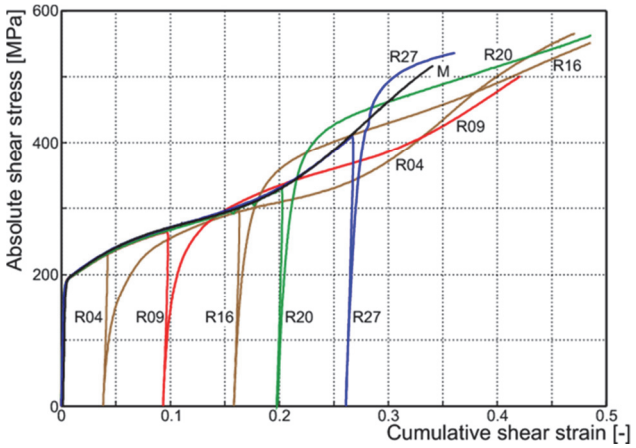

Fig. 2. Absolute stress versus cumulative strain during cyclic shear tests.

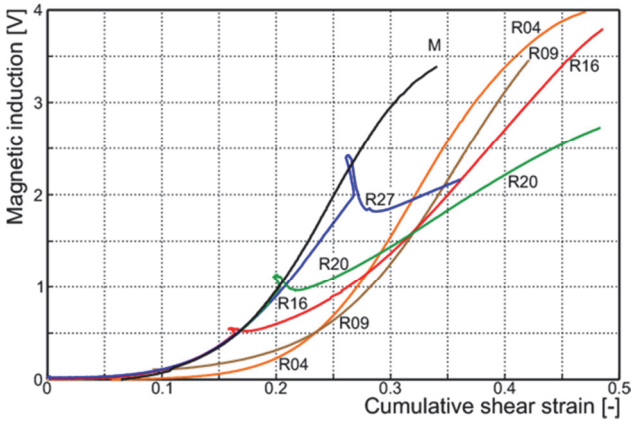

Fig. 3. Magnetic induction versus cumulative shear strain during cyclic shear tests.

In figure 3 the magnetic induction is plotted as a function of total accumulated strain. After strain reversal considerably more strain needs to be applied for the transformation to restart. Hamasaki et al. (2014) reported a similar stagnation of martensite transformation after strain reversal. In test R04 no martensite was formed before strain reversal. Yet, more plastic strain is needed to obtain a similar amount of martensite as in a monotonic test (M).

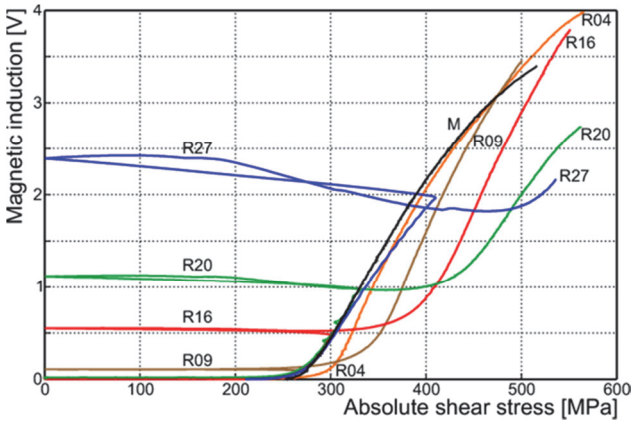

Fig. 4. Magnetic induction versus absolute stress during cyclic shear tests.

In figure 4 the magnetic induction is plotted against the cumulative absolute shear stress. The curve for test R04 now closely follows the monotonic test result. This indicates that the stress rather than the strain is driving the transformation. When more martensite has formed before strain reversal, again considerably more stress is required for martensite formation than before the strain path change. The reason for this is that the hard martensite already present in the material will carry a higher portion of the applied stress than the soft austenite. This effect is enhanced by the large Bauschinger effect which is present in the austenite. More stress must be applied to the phase mixture to raise the stress in the austenite to a level where transformation is induced again. This will be confirmed by the model calculations in section 5.

3.1. Stress partitioning

In figure 5 a detailed view of the induction voltage during stress reversal of test R20 is shown. It can be clearly seen, that the induction signal gradually rises when the stress drops from its maximum value of approximately 330 MPa. Maréchal et al. (2012) used this effect to calibrate the induction signal for the applied stress in tensile tests. With that result they estimated the value of the stress in the martensite fraction. They did this by removing the applied stress and measuring the value of the signal also at zero load.

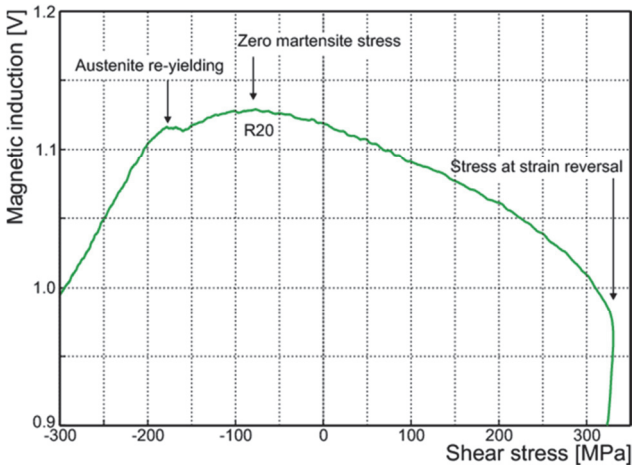

Fig. 5. *Magnetic induction versus stress during cyclic shear tests. Detail of test R20 in figure 4.*

Table 2. *Applied external stress and estimated martensite stress.*

test	applied strain	applied stress	martensite stress
R09	9.4%	265 MPa	280 MPa
R16	16.3%	300 MPa	360 MPa
R20	20.5%	330 MPa	410 MPa
xtra	24.0%	355 MPa	425 MPa
R27	27.0%	410 MPa	500 MPa

However, from our measurements it is apparent, that the induction signal keeps rising even after the applied stress has reached zero level and becomes negative. This indicates, that the stress in the martensite is actually higher than the overall applied stress. The actual level of the martensite stress can be estimated by determining the (negative) applied stress at which the induction signal reaches its maximum. Assuming both phases behave elastically during this phase of the stress reversal, the martensite stress can be estimated as the difference between the overall applied stress at reversal and the stress at maximum signal. For test R20 this is estimated as $\tau_{\alpha'} \approx 330 + 80 = 410$ MPa.

Note that this measurement is only possible in a shear test as the Villari effect is symmetric with respect to positive and negative values of the shear stress. No such symmetry exists with respect to tensile and compressive stresses. The martensite stresses estimated in this way are summarized in table 2. The 'xtra' entry is from a separate test shown in figure 7.

4. CONSTITUTIVE MODEL

The martensitic transformation is modeled as a stress-driven process similar to the model of Tamura (1982). It depends on the stress resolved in the austenite phase and it is determined as a function of the additional mechanical driving force supplied to the material as formulated by Patel and Cohen (1953). The model uses the Mean-Field homogenization method, which is based on the evolution of the average values of the field variables, stress and strain, in the constituting phases and the interactions between these average values. In this way it is possible to distinguish the stress in the phases from the overall applied stress. A detailed description of the complete model can be found in Perdahcıoğlu and Geijselaers (2012). A resume of it will be given in this section.

4.1. Martensite transformation model

The martensitic transformation involves a diffusion-less change of crystal structure. This was analyzed by Wechsler et al. (1953) and Bowles and MacKenzie (1954) starting from the postulate of an invariant plane (habit plane) as interface between the martensite and the parent austenite, where **n** is the normal to the habit plane. The deformation applied to the normal is described by the vector **m**. Due to lattice symmetry 24 different transformation systems (**n**, **m**) can be identified.

When a stress $\boldsymbol{\sigma}$ acts, while the transformation evolves, it supplies additional mechanical driving force U for the transformation (Patel & Cohen, 1953)

$$U = \boldsymbol{\sigma}_\gamma : (\mathbf{m} \otimes \mathbf{n}) = \boldsymbol{\sigma}_\gamma : \frac{1}{2}(\mathbf{m} \otimes \mathbf{n} + \mathbf{n} \otimes \mathbf{m}) \quad (1)$$

Here, $\boldsymbol{\sigma}_\gamma$ is the Cauchy stress in the austenite phase. In a polycrystalline material there are always some grains optimally oriented with respect to the local stress to maximize the mechanical driving force. Then, the maximum value of U is found as:

$$U^{\max} = \sum_j \sigma_{\gamma j} \lambda_j \quad (2)$$

where λ_j are the eigenvalues of the symmetric transformation deformation tensor (**m** ⊗ **n** + **n** ⊗ **m**)/2 and $\boldsymbol{\sigma}_{\gamma j}$ are the principal values of the local austenite stress tensor, both sorted in descending order (Geijselaers & Perdahcıoğlu, 2009).

The values of λ are material parameters, which are based on measured data such as transformation dilatation or crystal lattice constants. By XRD measurement the lattice parameters of both the aus-

tenite and the resulting bcc phases can be determined. With these data 24 transformation variants (n;m-pairs) can be calculated with respect to the austenite lattice along the procedures outlined by Wechsler et al. (1953) or Bowles and MacKenzie (1954). The resulting eigenvalues are given in table 3.

When the maximum supplied driving force $U^{\max}$ exceeds the required critical driving force ΔG^{cr} then according to Tamura (1982) the transformation will start. The required critical driving force ΔG^{cr} is the lumped value of a collection of separate energy terms such as chemical driving force, elastic energy, plastic dissipation, surface energy and interface mismatch energy.

Table 3. *Parameters for martensite transformation kinetics.*

λ_1	λ_2	λ_3	ΔG^{cr}	n	q	r
0.124	0.0	-0.104	56.5 MPa	2	0.5	2

The amount of martensite formed $f_{\alpha'}$ can be expressed as a monotonic function of $U^{\max}$ (Perdahcıoğlu and Geijselaers, 2012):

$$f_{\alpha'} = F(U^{\max}) = 1 - \sqrt[1-r]{1+(r-1)\left(\frac{\left\langle U^{\max} - \Delta G^{cr}\right\rangle}{q\Delta G^{ce}}\right)^{n}} \tag{3}$$

where n, r and q are parameters that determine the shape of the transformation curve. The values are obtained from fitting to the experimental results and are also given in table 3.

4.2. Mean-field modeling

The mean-field homogenization method is based on the evolution of the average values of the field variables in sub domains and the interactions between these average values. The overall stress $\boldsymbol{\sigma}$ and strain $\boldsymbol{\varepsilon}$ are related to the average stresses $\boldsymbol{\sigma}_\gamma$ and strains $\boldsymbol{\varepsilon}_\gamma$ in the austenite and $\boldsymbol{\sigma}_{\alpha'}$ and $\boldsymbol{\varepsilon}_{\alpha'}$ in the martensite by:

$$\begin{aligned}\boldsymbol{\sigma} &= (1-f_{\alpha'})\boldsymbol{\sigma}_\gamma + f_{\alpha'}\boldsymbol{\sigma}_{\alpha'}\\ \boldsymbol{\varepsilon} &= (1-f_{\alpha'})\boldsymbol{\varepsilon}_\gamma + f_{\alpha'}\boldsymbol{\varepsilon}_{\alpha'}\end{aligned} \tag{4}$$

It is assumed that the macroscopic stress-strain relation that is determined for an individual phase is also valid as an average stress average strain relation for that phase within the compound:

$$\dot{\boldsymbol{\sigma}}_\gamma = \mathbb{C}_\gamma : \mathbf{D}_\gamma;\ \dot{\boldsymbol{\sigma}}_{\alpha'} = \mathbb{C}_{\alpha'} : \mathbf{D}_{\alpha'} \tag{5}$$

where $\mathbf{D}_{\gamma,\alpha'}$ is the average strain rate in the respective phase and $\mathbb{C}_{\gamma,\alpha'}$ is the consistent fourth order elasto-plastic tangent of the phase. The constitutive model used here is Chaboche (1986) kinematic hardening. The data used in the model are summarized in appendix A.

To close the set of equations the relation between average phase strain rates $\mathbf{D}_i$ and the overall strain rate $\mathbf{D}$ has to be specified through fourth order strain concentration tensors $\mathbb{A}_{\gamma,\alpha'}$ (Hill, 1965):

$$\mathbf{D}_\gamma = \mathbb{A}_\gamma : \mathbf{D};\ \mathbf{D}_{\alpha'} = \mathbb{A}_{\alpha'} : \mathbf{D} \tag{6}$$

which, by virtue of equation (4), are subject to:

$$(1-f_{\alpha'})\ \mathbb{A}_\gamma + f_{\alpha'}\mathbb{A}_{\alpha'} = \mathbb{I} \tag{7}$$

where $\mathbb{I}$ is the symmetric fourth order unit tensor.

Different schemes have been formulated using specific definitions of $\mathbb{A}$. Here we use an approximation to the self consistent scheme by Lielens et al. (1998), the so called double inclusion scheme, see also Doghri and Ouaar (2003) or Perdahcıoğlu and Geijselaers (2010). It is derived by interpolating between two variants of the Mori and Tanaka (1973) scheme with the roles of both phases as matrix and inclusion interchanged. For the Mori-Tanaka model with martensite as inclusion in austenite and the other way around we can write:

$$\begin{aligned}\mathbf{D}_{\alpha'} &= \mathbb{H}_{\alpha'} : \mathbf{D}_\gamma\\ \mathbf{D}_\gamma &= \mathbb{H}_\gamma : \mathbf{D}_{\alpha'} \rightarrow \mathbf{D}_{\alpha'} = \mathbb{H}_\gamma^{-1} : \mathbf{D}_\gamma\end{aligned} \tag{8}$$

where $\mathbb{H}_i$ is the 'local' strain concentration tensor for the strain in the inclusion i with respect to that in the matrix $\mathbf{m}$. $\mathbb{H}_i$ is calculated as:

$$\mathbb{H}_i = (\mathbb{I} - \mathbb{S}_m : (\mathbb{I} - \mathbb{C}_m^{-1} : \mathbb{C}_i))^{-1} \tag{9}$$

where $\mathbb{S}_m$ is the Eshelby tensor of the matrix:

$$\mathbb{S}_m = \frac{3\kappa_m}{3\kappa_m + 4\mu_m}\mathbb{I}^{v} + \frac{6}{5}\frac{\kappa_m + 2\mu_m}{3\kappa_m + 4\mu_m}\mathbb{I}^{d} \tag{10}$$

where $\mathbb{I}^{v}$ and $\mathbb{I}^{d}$ are the fourth order volumetric and deviatoric unit tensors. The bulk modulus κ and the shear modulus μ are found from an isotropic projection of the elasto-plastic constitutive tensor:

$$3\kappa_m = \mathbb{C}_m :: \mathbb{I}^{v};\ 10\mu_m = \mathbb{C}_m :: \mathbb{I}^{d} \tag{11}$$

From the interpolated local concentration tensor $\mathbb{H}^*_{\alpha'}$

$$\mathbb{H}^*_{\alpha'} = (f_{\alpha'}\mathbb{H}_{\alpha'}^{-1} + (1 - f_{\alpha'})\mathbb{H}_\gamma)^{-1} \tag{12}$$

with the help of equation (7), the strain concentration tensors with respect to the global strain are calculated

$$\mathbb{A}_\gamma = ((1 - f_{\alpha'})\mathbb{I} + f_{\alpha'}\mathbb{H}^*_{\alpha'})^{-1}$$
$$\mathbb{A}_{\alpha'} = \mathbb{H}^*_{\alpha'} : \mathbb{A}_\gamma \qquad (13)$$

4.3. Mean-field model with phase transformation

To obtain a homogenized stress-strain relation the deformation rate is partitioned into an elastic rate $\mathbf{D}^e$, a plastic deformation rate $\mathbf{D}^p$ and a transformation plasticity rate $\mathbf{D}^{tr}$ (Kubler et al., 2011), of which the elastic plus plastic rate is partitioned among the phases:

$$\mathbf{D}_{\gamma,\alpha'} = \mathbf{D}^e_{\gamma,\alpha'} + \mathbf{D}^p_{\gamma,\alpha'} = \mathbb{A}_{\gamma,\alpha'} : (\mathbf{D} - \mathbf{D}^{tr}) \qquad (14)$$

Differentiation of the stress as defined in equation (4) yields:

$$\dot{\boldsymbol{\sigma}} = (1 - f_{\alpha'})\dot{\boldsymbol{\sigma}}_\gamma + f_{\alpha'}\dot{\boldsymbol{\sigma}}_{\alpha'} + \dot{f}_{\alpha'}(\boldsymbol{\sigma}_{\alpha'} - \boldsymbol{\sigma}_\gamma) \qquad (15)$$

The consequence of the last term in the right hand side of this equation would be that newly formed martensite gets the same stress as the already formed martensite. A more realistic assumption is to assign to pristine martensite the stress of the parent austenite and add this as a dilution term to the martensite stress rate:

$$\dot{\boldsymbol{\sigma}}_{\alpha'} = \mathbb{C}_{\alpha'} : \mathbf{D}_{\alpha'} + \frac{\dot{f}_{\alpha'}}{f_{\alpha'}}(\boldsymbol{\sigma}_\gamma - \boldsymbol{\sigma}_{\alpha'}) \qquad (16)$$

Substitution of equation (14) into (16) and of the result into equation (15) yields:

$$\dot{\boldsymbol{\sigma}} = ((1 - f_{\alpha'})\mathbb{C}_\gamma : \mathbb{A}_\gamma + f_{\alpha'}\mathbb{C}_{\alpha'} : \mathbb{A}_{\alpha'}) : (\mathbf{D} - \mathbf{D}^{tr}) \qquad (17)$$

The transformation plasticity depends on the transformation rate:

$$\mathbf{D}^{tr} = \mathbf{T}\,\dot{f}_{\alpha'} \qquad (18)$$

where $\mathbf{T}$ is the second order transformation plasticity tensor, which can be expressed as a function of U^{max} (Perdahcıoğlu & Geijselaers, 2012). An implicit equation for the transformation rate is found by differentiation of equation (3) and substitution of equations (14) and (18):

$$\dot{f}_{\alpha'} = F' \frac{\partial U^{max}}{\partial \boldsymbol{\sigma}_\gamma} : \mathbb{C}_\gamma : \mathbb{A}_\gamma : (\mathbf{D} - \mathbf{T}\,\dot{f}_{\alpha'}) \qquad (19)$$

Solving for $\dot{f}_{\alpha'}$ yields an explicit expression:

$$\dot{f}_{\alpha'} = \frac{F' \dfrac{\partial U^{max}}{\partial \boldsymbol{\sigma}_\gamma} : \mathbb{C}_\gamma : \mathbb{A}_\gamma}{1 + F' \dfrac{\partial U^{max}}{\partial \boldsymbol{\sigma}_\gamma} : \mathbb{C}_\gamma : \mathbb{A}_\gamma : \mathbf{T}} : \mathbf{D} \qquad (20)$$

After combining (20) with (18) and (14) and substitution into (17), the stress-strain response for the homogenized material including transformation plasticity is obtained as:

$$\dot{\boldsymbol{\sigma}} = \sum_{i=\gamma,\alpha'} f_i \, \mathbb{C}_i : \mathbb{A}_i : \left(\mathbb{I} - \frac{F'\mathbf{T} \otimes \dfrac{\partial U^{max}}{\partial \boldsymbol{\sigma}_\gamma} : \mathbb{C}_\gamma : \mathbb{A}_\gamma}{1 + F' \dfrac{\partial U^{max}}{\partial \boldsymbol{\sigma}_\gamma} : \mathbb{C}_\gamma : \mathbb{A}_\gamma : \mathbf{T}} \right) : \mathbf{D} \qquad (21)$$

This material tangent describes the constitutive behavior of the austenitic steel including the phase transformation and transformation plasticity. Also the tension-compression asymmetry of the mechanical response is included. The driving force for transformation differs between tension and compression due to the difference of the positive and negative eigenvalues of the transformation strain.

5. SIMULATION RESULTS

The parameters for the cyclic stress strain behaviour of both austenite and martensite as used in the simulations are summarized in table 4. The austenite is modeled with a pronounced Bauschinger effect, whereas this is kept to a modest level in martensite. The parameters describing the transformation are given in table 3. All parameters have been optimized to fit the simulation results to the measurements.

5.1. Cyclic stress-strain and transformation response

In figure 6 the simulated stress-strain response is plotted, together with the measured behavior. The correspondence is very good over the whole range of strains in the monotonic behavior as well as in the reversed shear response. This also holds for the 'unfinished' cyclic test as shown in figure 7.

In figure 8 the phase fraction as a function of cumulative strain is shown. Comparison with figure 3 shows that the main characteristics are largely reproduced. In test R04 very little martensite was pro-

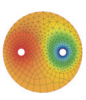

duced before strain reversal, yet after reversal

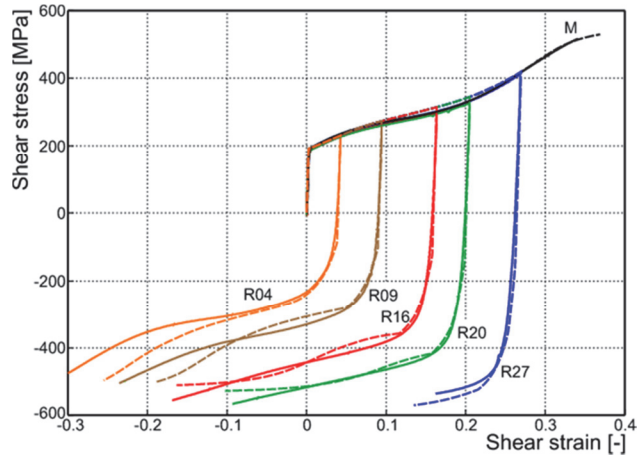

Fig. 6. Stress versus strain during cyclic shear tests, comparison of measurements and simulations (dashed).

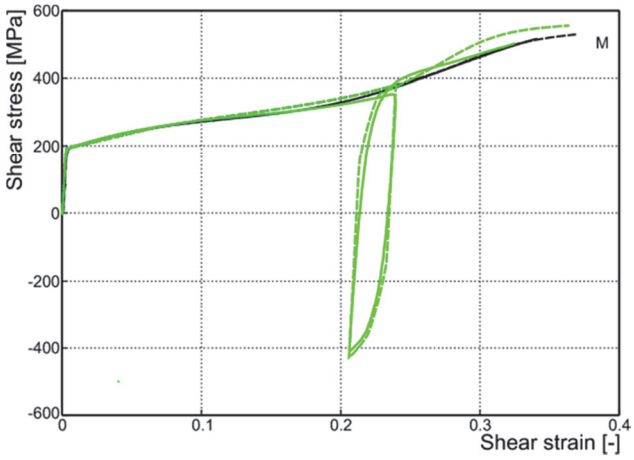

Fig. 7. Stress versus strain during 'xtra' cyclic test, comparison of measurements and simulations (dashed).

extra strain needs to be applied to obtain a comparable amount of martensite. In all tests where martensite was formed before strain reversal, a stagnation of the transformation is observed after reversal. After strain reversal additional strain must be applied to restart the transformation. This is caused by the Bauschinger effect of the austenite stress-strain response. More strain is required to raise the stress in the austenite to the level before strain reversal. The stress in the austenite determines the transformation. In figure 9 the phase fraction as a function of applied stress is shown. Also here comparison with figure 4 shows that the applied stress needed for transformation in test R04 closely follows the stresstransformation curve of the monotonic test. In all tests where martensite was formed before strain reversal, after strain reversal more stress than before reversal needs to be applied to restart the transformation. The reason for this is that the applied stress is partitioned among both phases. The hard martensite will tend to carry more stress than the soft austenite. The stress in the austenite is considerably lower than the externally applied stress.

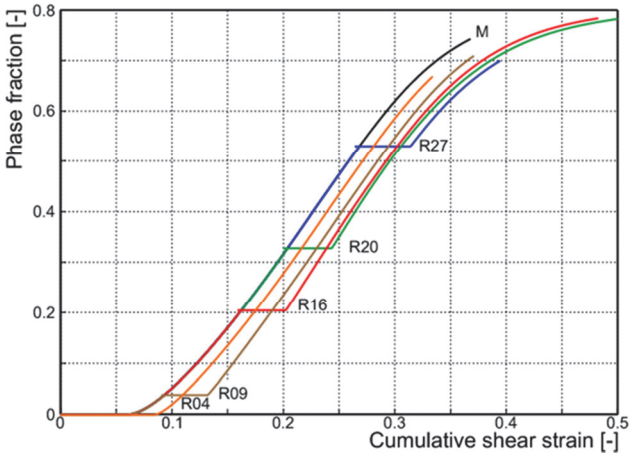

Fig. 8. Simulated martensite phase fraction versus absolute cumulative strain during cyclic shear.

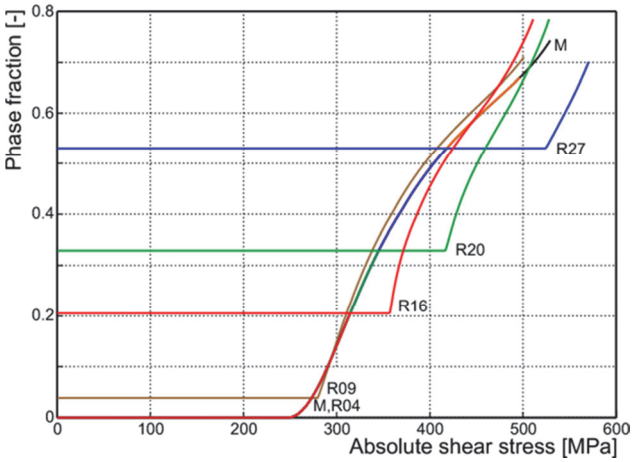

Fig. 9. Simulated martensite phase fraction versus absolute stress during cyclic shear.

5.2. Stress partitioning

On account of equation (16), in the calculations the first formed martensite has an average stress equal to that of austenite. The higher stiffness of the martensite compared to that of the austenite causes stress concentration in the martensite, the average stress in the martensite quickly rises. This is shown in figure 10. The calculated stress in the martensite compares well with the values of the stress in the martensitic phase determined from the analysis of the magnetic induction signal as explained in section 3 and summarized in table 2.

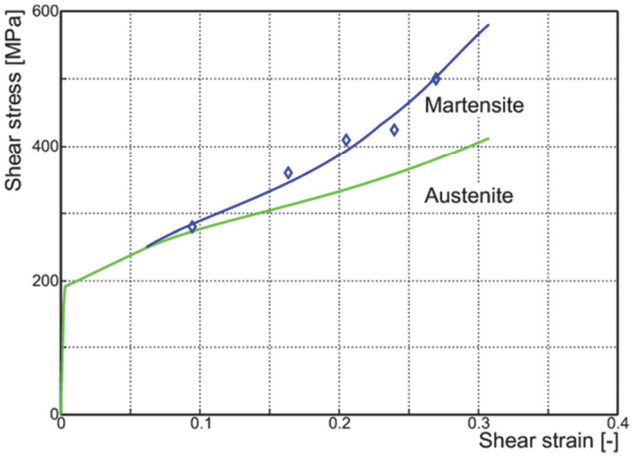

Fig. 10. *Partitioning of the average phase stresses. Diamonds indicate measured martensite stress (table 2).*

6. CONCLUSIONS

A 12Cr9Ni4Mo austenitic stainless steel has been subjected to cyclic shear tests. This steel transforms to martensite when subjected to mechanical working. During the tests, apart from the stress and strain also the magnetic induction has been measured to monitor the course of the transformation. From the magnetic induction signal after strain reversal the partitioning of the shear stress among both phases can be estimated.

To represent the material behavior of this steel a model can be used in which i) the martensite transformation is modeled as a stress-induced transformation, where the stress in the austenite phase is assumed to drive the transformation, ii) the stress-strain response of the austenite is characterized by a strong Bauschinger effect and iii) both phases, austenite and martensite are modeled individually and are combined through a mean-field homogenization method.

This way an excellent fit of the stress-strain response is obtained. This applies to the stress during a monotonic deformation as well as to the stress level after strain reversal. The model also reproduces accurately the stress partitioning among the phases as estimated from the magnetic induction signal. The simulated transformation as function of both stress and strain displays the main characteristics that are found in the measurements.

ACKNOWLEDGEMENT

This research was carried out under project number M63.1.09373 in the framework of the Research Program of the Materials innovation institute M2i (www.m2i.nl).

APPENDIX A. MATERIAL PARAMETERS FOR KINEMATIC HARDENING

Both austenite and martensite are modeled as kinematic hardening with Chaboche back stress evolution and a Voce law for the yield surface radius.

The elasto-plastic behavior of phase i can be described by the yield condition:

$$\frac{3}{2}(\mathbf{S}_i - \mathbf{X}_i) : (\mathbf{S}_i - \mathbf{X}_i) - R_i^2(p_i) = 0 \qquad (22)$$

where $\mathbf{S}_i$ is the deviatoric stress and $\mathbf{X}_i$ the back stress in the phase, R_i is the radius of the yield surface, which depends on the equivalent plastic strain p_i. Armstrong and Frederick (1966) formulated an evolution equation for the back stress, which was extended by Chaboche (1986) to:

$$\dot{\mathbf{X}}_i = \sum_j \dot{\mathbf{X}}_{ij} = \sum_j (h_{ij} D_i^{\mathrm{P}} - c_{ij} \mathbf{X}_{ij} \dot{p}_i) \qquad (23)$$

A Voce-type law is used for the yield surface radius $R_i(p_i)$:

$$R_i(p_i) = R_i^0 + \sum_j \Delta R_{ij} (1 - \mathrm{e}^{-r_{ij} p_i}) \qquad (24)$$

The parameters used in the simulations are summarized in table 4.

Table 4. *Material properties for austenite and martensite.*

	austenite	martensite
R_i^0 (MPa)	331	750
ΔR_{ij} (MPa)	-75 1710 -180	96
r_{ij}	104 1.8 1.3	49
h_{ij} (GPa)	9 0.27	180
c_{ij}	104 1.3	33.2

REFERENCES

Armstrong, P. J., Frederick, C. O., 1966, A Mathematical Representation of the Multiaxial Bauschinger Effect, Tech. Rep. RD/B/N 731, CEGB.

Berrahmoune, M. R., Berveiller, S., Inal, K., Patoor, E., 2006, Delayed Cracking in 301LN Austenitic Steel after Deep Drawing: Martensitic Transformation and Residual

Stress Analysis, Mat Sci Eng A-Sruct, 438-440, 262–266.
Bowles, J. S., MacKenzie, J. K., 1954, The Crystallography of Martensitic Transformations I and II, Acta Metall Mater, 2, 129–147.
Chaboche, J. L., 1986, Time Independent Constitutive Theories for Cyclic Plasticity, Int J Plasticity, 2, 149–188.
Delannay, L., Jacques, P. J., Pardoen, T., 2008, Modelling of the Plastic Flow of TRIP-Aided Multiphase Steel Based on an Incremental Mean-Field Approach, Int J Solids Struct, 45, 1825–1843.
Diani, J. M., Parks, D. M., 1998, Effects of Strain State on the Kinetics of Strain-Induced Martensite in Steels, J Mech Phys Solids, 46, 1613–1635.
Doghri, I., Ouaar, A., 2003, Homogenization of Two-Phase Elasto-Plastic Composite Materials and Structures: Study of Tangent Operators, Cyclic Plasticity and Numerical Algorithms, Int J Solids Struct, 40, 1681–1712.
Gallée, S., Manach, P. Y., Thuillier, S., 2007, Mechanical Behavior of a Metastable Austenitic Stainless Steel under Simple and Complex Loading Paths, Mat Sci Eng A-Sruct, 466, 47–55.
Geijselaers, H. J. M., Perdahcıoğlu, E. S., 2009, Mechanically Induced Martensitic Transformation as a Stress Driven Process, Scripta Mater, 60, 29–31.
Hallberg, H., Håkansson, P., Ristinmaa, M., 2007, A Constitutive Model for the Formation of Martensite in Austenitic Steels under Large Strain Plasticity, Int J Plasticity, 23, 1213–1239.
Hamasaki, H., Ishimaru, E., Yoshida, F., 2014, Cyclic Stress-Strain Response and Martensite Transformation Behavior for Type 304 Stainless Steel, Appl Mech Mater, 510, 114–117.
Han, H. N., Lee, C. G., Oh, C. S., Lee, T.-H., Kim, S. J., 2004, A Model for Deformation Behavior and Mechanically Induced Martensitic Transformation of Metastable Austenitic Steel, Acta Mater, 52, 5203–5214.
Hill, R., 1965, A Self-Consistent Mechanics of Composite Materials, J Mech Phys Solids, 13, 213–222.
Kubler, R. F., Berveiller, M., Buessler, P., 2011, Semi Phenomenological Modelling of the Behavior of TRIP Steels, Int J Plasticity, 27, 299–327.
Lani, F., Furnémont, Q., Van Rompaey, T., Delannay, F., Jacques, P. J., Pardoen, T., 2007, Multiscale Mechanics of TRIP-Assisted Multiphase Steels: II. Micromechanical Modelling, Acta Mater, 55, 3695–3705.
Lebedev, A. A., Kosarchuk, V. V., 2000, Influence of Phase Transformations on the Mechanical Properties of Austenitic Stainless Steels, Int J Plasticity 16, 749–767.
Lielens, G., Pirotte, P., Couniot, A., Dupret, F., Keunings, R., 1998, Prediction of Thermo-Mechanical Properties for Compression Moulded Composites, Compos Part A-Appl S, 29, 63–70.
Maréchal, D., Sinclair, C. W., Dufour, P., Jacques, P. J., Mithieux, J.-D., 2012, In-Situ Measurements of Load Partitioning in a Metastable Austenitic Stainless Steel: Neutron and Magnetomechanical Measurements, Metall Mater Trans A, 43, 4601–4609.
Mori, T., Tanaka, K., 1973, Average Stress in Matrix and Average Elastic Energy of Materials with Misfitting Inclusions, Acta Metall Mater 21, 571–574.
Nagy, E., Mertinger, V., Tranta, F., Sólyom, J., 2004, Deformation Induced Martensitic Transformation in Stainless Steels, Mat Sci Eng A-Sruct, 378, 308–313.
Olson, G. B., Cohen, M., 1975, Kinetics of Strain-Induced Martensitic Nucleation, Metall Trans A, 6, 791–795.
Patel, J. R., Cohen, M., 1953, Criterion for the Action of Applied Stress in the Martensitic Transformation, Acta Metall Mater, 1, 531–538.
Perdahcıoğlu, E. S., Geijselaers, H. J. M., 2010, Constitutive Modeling of Two Phase Materials Using the Mean Field Method for Homogenization, International Journal of Materials Forming, 4, 93–102.
Perdahcıoğlu, E. S., Geijselaers, H. J. M., 2012, A Macroscopic Model to Simulate the Mechanically Induced Martensitic Transformation in Metastable Austenitic Stainless Steels, Acta Mater, 60, 4409–4419.
Perdahcıoğlu, E. S., Geijselaers, H. J. M., Groen, M., 2008a, Influence of Plastic Strain on Deformation-Induced Martensitic Transformations, Scripta Mater, 58, 947–950.
Perdahcıoğlu, E. S., Geijselaers, H. J. M., Huétink, J., 2008b, Influence of Stress State and Strain Path on Deformation Induced Martensitic Transformations, Mat Sci Eng A-Sruct, 481-482, 727–731.
Post, J., Nolles, H., Datta, K., Geijselaers, H. J. M., 2008, Experimental Determination of the Constitutive Behaviour of a Metastable Austenitic Stainless Steel, Mat Sci Eng A-Sruct, 498, 179–190.
Spencer, K., Conlon, K. T., Bréchet, Y., Embury, J. D., 2009, The Strain Induced Martensite Transformation in Austenitic Stainless Steels Part 2 - Effect of Internal Stresses on Mechanical Response, Mater Sci Tech Ser, 25, 18–28.
Stringfellow, R. G., Parks, D. M., Olson, G. B., 1992, A Constitutive Model for Transformation Plasticity Accompanying Strain Induced Martensitic Transformations in Metastable Austenitic Steels, Acta Metall Mater, 40, 1703–1716.
Tamura, I., 1982, Deformation Induced Martensitic Transformation and Transformation Induced Plasticity in Steels, Met Sci, 16, 245–254.
Tomita, Y., Iwamoto, T., 1995, Constitutive Modelling of TRIP Steel and its Application to the Improvement of Mechanical Properties, Int J Mech Sci, 37, 1295–1305.
Venables, J. A., 1962, The Martensite Transformation in Stainless Steel, Philos Mag, 7, 35–44.
Wechsler, M. S., Lieberman, D. S., Read, T. A., 1953, On the Theory of the Formation of Martensite, AIME Transactions Journal of Metals, 197, 1503–1515.

ZACHOWANIE SIĘ BLACH Z AUSTENITYCZNEJ STALI NIERDZEWNEJ PODDAWANYCH CYKLICZNYM OBCIĄŻENIOM ŚCINAJĄCYM

Streszczenie

Próbki z austenitycznej stali nierdzewnej poddawano odkształceniom o dużej amplitudzie i przeciwnych zwrotach. W przeprowadzonych doświadczeniach, poza pomiarem naprężenia i odkształcenia, mierzono również indukcję magnetyczną do monitorowania przemiany austenitu w martenzyt. Dzięki bezpośrednim pomiarom indukcji magnetycznej możliwe było oszacowanie wielkości naprężenia w poszczególnych fazach materiału.

Przy małych odkształceniach, dla przeciwnego zwrotu, obserwowany jest klasyczny efekt Bauschingera. Gdy dokonywana jest zmiana zwrotu przy większych odkształceniach, mierzone naprężenie jest większe niż przed zmianą. Obserwowana jest

również stagnacja przemiany fazowej, to znaczy, że potrzebne jest wyższe odkształcenie i naprężenie niż przed zmianą ścieżki odkształcania aby ponownie zaczęła się przemiana po zmianie. Zaobserwowane zachowanie można opisać modelem, w którym dla przemiany martenzytycznej ma zastosowanie model naprężenia indukowanego przemianą.

Zachowanie konstytutywne austenitu i martenzytu zostało opisane modelem Chaboche'a uwzględniającym efekt Bauschingera. W modelu wykorzystano metodę homogenizacji dla opisu materiału i faz, otrzymując konstytutywny model zachowania się dwu-fazowego kompozytu. Przyłożone naprężenie, naprężenie w fazie martenzytu i obserwowane zachowanie się podczas przemiany w trakcie cyklicznego ścinania zostało bardzo dobrze odtworzone w symulacjach modelu.

Received: November 10, 2014
Received in a revised form: November 17, 2014
Accepted: November 17, 2014